Optical and Quantum Electronics (2006) 38:993–1004
DOI 10.1007/s11082-006-9051-7

Simulation of carrier injection and propagation in molecularly disordered systems

GREGOR MELLER*, LING LI, STEFAN HOLZER AND HANS KOSINA
Institute for Microelectronics, TU Wien, Gußhausstraße 27-29/E360, 1040 Wien, Austria
*(*author for correspondence: E-mail: meller@iue.tuwien.ac.at).*

Received: 2 September 2006; Accepted: 26 November 2006

Abstract. Simulations permit the modification of the physical parameters of a system even when the corresponding experiments would lead to operationally untractable demands. This work discusses the application of the Kinetic Monte Carlo method to the numerical investigation of interface and bulk effects in pure amorphous Zinc Phthalocyanine films. Electrical currents in a single-layer opto-electronic device are studied under varying physical conditions and compared with empirical data.

Key words: kinetic monte carlo, organic semiconductors, zinc phthalocyanine

1. Introduction

Dangling π and π^* orbitals of unsaturated polymers can overlap to form conduction bands for electrons and holes, respectively. Since polymers are constituted by van der Waals-forces they form soft, and hence easy to polarize, lattices which are locally distortable even under the influence of a single electron's Coulomb potential. The resulting confined *polaronic* motion of an electron with its corresponding topological defect dresses the particle's effective mass and energy and is the physical origin of a variety of temperature and field activated, barrier-crossing transport regimes ranging from incoherent thermally assisted tunneling to bandlike small polaron transport. The relative importance assigned to a polaron's constituents and transport mechanisms determines the conduction regime occurring in a certain compound. This regime depends both on the system's chemistry and degree of molecular ordering. For example, the mobility of charge carriers in amorphous organic materials such as Peierl's-distorted conjugated hydro-carbon chains or samples doped with molecules acting as shallow and therefore thermally excitable traps, is typically several orders of magnitude lower than that in inorganic crystals. The interplay of different charge transfer mechanisms with specific properties of the

branched molecular π and π^* wave functions can be utilized to govern a sample's electrical characteristics. This opens the opportunity to promising applications.

Organic opto-electronic devices are assemblies of about 100 nm thin amorphous or polycrystalline functional layers operating at an electric field strength of the order of 1 MV/cm. The physical phenomena determining a device's electrical characteristics include charge injection and transport, exciton creation, electron-hole recombination and trapping.

The outline of this paper is as follows: first, a brief overview of the simulation technique and the device-related assumptions are given. Then, the underlying physical models and the simulation algorithm are presented. Finally, we provide the simulation results and discuss how they relate to reality.

2. Kinetic Monte Carlo simulations

To study both the static and the dynamic electrical properties of a conductive organic film simultaneously, a three-dimensional Kinetic Monte Carlo (KMC) simulator has been developed. KMC bridges the gap between molecular dynamics and ensemble Monte Carlo (MC) methods for rare event systems. The Molecular Dynamics method models the dynamics deterministically as a causal sequence of configurations derived from the particles' equations of motion. However, for large systems or computationally demanding energy landscapes the time scale of Molecular Dynamics is limited to 10^{-9}–10^{-12} s. On the other hand, the phase-space traversal of ensemble MC techniques, although evolving towards the state of lowest free energy in accordance with the laws of thermodynamics, does not describe how the system approaches its steady state in a chronological sense and thus cannot correctly account for a system's non-stationary observables. By assigning an individual time scale to each electron transition, KMC enables a kinetic, i.e., rate-based description of the system's evolution from state to state over long time scales on the time scales of temperature and field activated molecular oxidation and reduction events. The algorithm's flow chart is described by Fig. 1. A KMC implementation either belongs to the class of *Random Selection Methods* or to the somewhat more deterministic class of *First Reaction Methods*. Their main difference is the way in which the importance sampling (bold box) is based on the events' time-scales. In this work, the First Reaction Method was considered, i.e., the system's time evolution is triggered by the electron whose residency time is elapsed next.

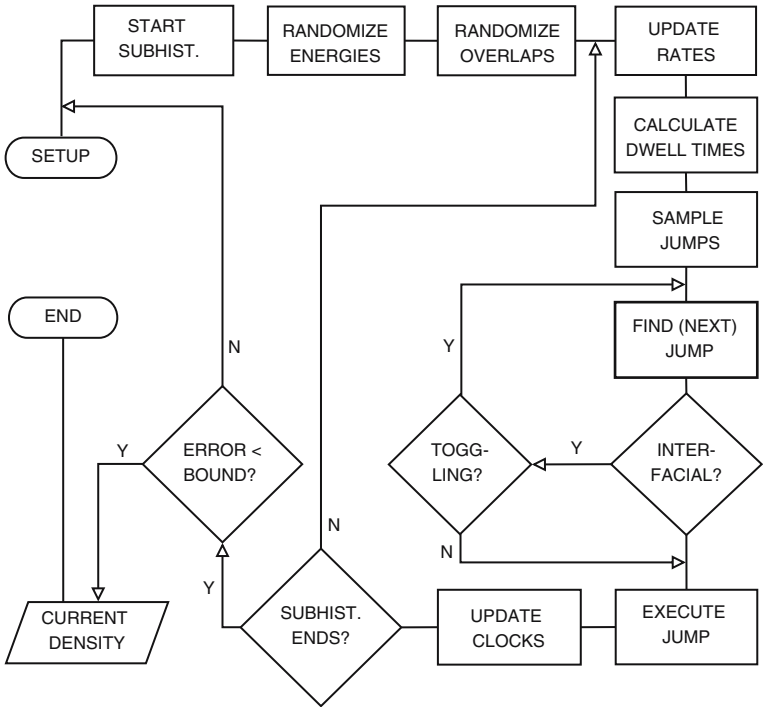

Fig. 1. The simulator's flow chart.

3. Physical assumptions

Due to the high bandgap ($\approx 3\,\mathrm{eV}$) of π-conjugated systems, the probability for the thermal generation of free carriers at room temperature is vanishing. As a consequence of the resulting lack of intrinsic carriers, not only plays the propagation but also the injection of currents into a polymer's conduction band a pre-eminent role in the performance of an organic opto-electronic device. For being successfully injected into a n-conductive assembly, an electron has either to cross the maximum of the rounded triangular potential barrier at the cathode by thermal activation or to tunnel through it (Fig. 2(a)). Subsequently, the electron experiences a driven random walk through the bulk's random energy landscape which is biased by the applied electric field. The carrier is finally absorbed at the anode affected by an interfacial potential, which is essentially coined by surface charges influenced in the contact.

In the absence of strong correlations, the polarization energies and thus the molecular energy spectra depend on a large number of *mutually independent* random variables. According to the Central Limit Theorem they thus form a Gaussian density of states (DOS) reflecting the system's degree

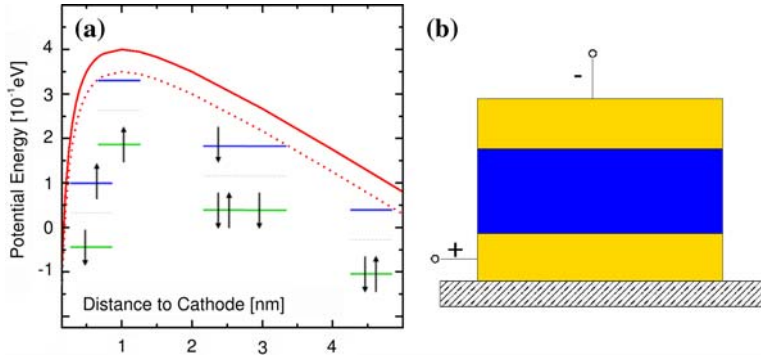

Fig. 2. (a) Depicts the implementation of the molecules as fermion reservoirs and the bonding and antibonding DOS at the organo-metallic interface. Due to the low value of ϵ_r, the Coulombic image force potential reduces the injection barrier for both free electrons in the LUMO and holes in the HOMO-level significantly. Interband tunneling between π and π^* states is allowed, intramonomer transitions, however have been neglected. (b) The simulated single layer device.

of *energetic disorder*, i.e., its susceptibility to traps (Bässler 1993). The resulting barriers are mirrored in the transport's activated nature and prevent the electrons from being delocalized. Energetic disorder, in other words, defeats the existence of bands. The π and π^* carriers do not possess a non-zero velocity distribution and the mean free path equals the intermolecular distance (Schwoerer and Wolf 2005). Consequently, the electric potentials of these carriers equal that of screened, seldomly displaced point charges and cannot be viewed as a perturbation like in conventional band theories. The polymer's monomers, oligomers or chain segments are being charged and discharged by instantaneous tunneling events. In contrast to the multiple trapping picture (Noolandi 1977), there is no diffusive or band-like motion assumed to take place between the electron's capture and release. Hence, the only non-zero contribution to the transfer's duration is the *dwell time* an electron has to reside on a molecule until it is activated by a sufficiently energetic phonon. The resulting retardation is occasionally the source of dispersive behavior, where neither the mobility nor the diffusion constant can be uniquely defined. Trapping, on the contrary, is usually assumed to be an unactivated process, independent from the transition's final energy, as well as from the temperature and the applied electric field. In other words, there are two different conduction mechanisms of different effectiveness involved.

4. Physical models

As a representative organic assembly, the undoped single-layer device Au/ZnPc/Au exhibits contact-dominated behavior and thus was simulated

in-situ. Fabrication-induced effects like the diffusion of metal atoms into the bulk were disregarded. Generally, the cathode and the anode were treated equivalently, ignoring the device's asymmetry originating from the manufacturing process of organic-on-metal and metal-on-organic interfaces (Fig. 2(b)).

4.1. SIMULATION OF THE CARRIER DYNAMICS

The emission and absorption of electrons at the contacts, which were modeled as plain organo-metallic heterojunctions, was seamlessly included into the simulation of the bulk dynamics by the use of a joint transition rate ruling events with time scales varying over several orders of magnitude. As suggested by Wolf *et al.* (1999), the recombination of the electrons with their image charges at the cathode was excluded for performance reasons. To capture sample-dependent properties like boundary and surface effects, periodic boundary conditions were not used.

According to Fichthorn and Weinberg (1991) a MC simulation ruled by a master equation and thus by transition rates obeying the principle of *microscopic reversibility* or *detailed balance*, can be related to Poisson-like processes if the following three criteria are met: (i) the transition probabilities reflect a dynamical hierarchy ranking the occurrence of processes, (ii) the time increments upon successful events are formulated correctly in term of the microscopic kinetics, and (iii) the events must be effectively independent from each other. All three criteria are met for the Abrahams–Miller rate, which approximates the single phonon absorption probability by a Boltzmann factor.

$$\nu_{ij} = \nu_0 \exp\left[-2\gamma a \frac{R_{ij}}{a}\right] \times \begin{cases} \exp\left[-\frac{\epsilon_j - \epsilon_i}{k_B T}\right] & \text{for} \quad \epsilon_j > \epsilon_i \\ 1 & \text{for} \quad \epsilon_j < \epsilon_i \end{cases} \tag{1}$$

Here, ν_0 denotes the *attempt-to-escape frequency*, the *conjugation factor* γ describes the wave-function's spacial decay, a is the average lattice constant, ϵ_i and ϵ_j are the site-energies, and R_{ij} is their mutual distance. The Abrahams–Miller rate obeys the principle of detailed balance and thus drives the system *ergodically* towards its state of least free energy. Mathematically this means, that an observable's temporal average converges towards the exact ensemble expectation value. Alternatively, ergodicity can be characterized by a non-vanishing transition probability for any pair of system states.

The semiconductor's loss of long-range order is cast into the carrier waiting time distribution which establishes a dynamical hierarchy of the processes based on their respective time-scale. The expectation value of the

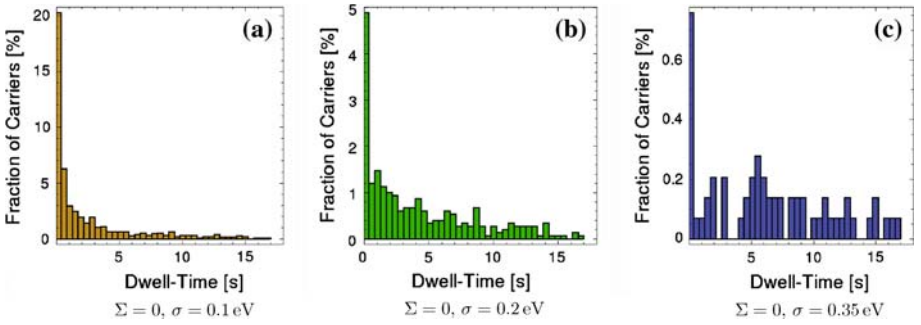

Fig. 3. Waiting time distributions of approximately 1500 π-electrons for various degrees of energetic disorder σ at vanishing spacial disorder Σ.

dwell time at a site i depends on the hop-off counter-probability and reads as

$$\langle \tau^i \rangle = \left(\sum_{j \neq i} \nu_{ij} \right)^{-1} . \tag{2}$$

The resulting long-tailed waiting time distributions (Figs. 3(a)–(c)) account for the fact that there are much faster and much slower events than average. As the figures show, the distribution tail is enhanced for increasing energetic variance. The basis for an importance sampling is to use an event's time-scale as a ranking criterion. The accuracy of $\langle \tau^i \rangle$ is limited by the rate theory used and by the approximation of the rate constants by independent Poisson processes.

The Abrahams–Miller expression is not the most physically sophisticated choice for KMC, however it is the simplest one. It represents a zero-order approximation for the non-equilibrium dynamics, since multiphonon-processes and thus the appearance of intermediate states are neglected. Consequently, the stochastic delay assigned to an exothermic event is neither assumed to be reduced by an applied electric field nor to be inversely proportional to the transition's heat effect. The Abrahams–Miller rate may only be applied under certain conditions: (i) the morphologic phase is *unconjugated*, i.e., the molecules' electronic spectra are too different to enable carrier delocalization, (ii) the phonon energy does not exceed the thermal energy and, (iii) the molecules are so weakly coupled, that both charging and discharging are *non-adiabatic* processes. In other words, it is assumed that the electrons cannot follow the fast atomic motions and hence react to energetic advantages due to configurational changes in the polymer backbone only casually.

When simulating on a microscopic time-scale, no two events may happen simultaneously. KMC triggers the system's time-evolution with the

fastest event. Basing a simulation on the Abrahams–Miller expression means to model the driven carrier gases dynamics on the time-scales of phonon-assisted tunneling. On this time-scale, simultaneous charge transfer might well happen.

Each orbital is assigned a *private clock* which is zeroed when this orbital is charged. The difference Δt between a carrier's dwell-time and its private clock measures the fraction of the dwell-time elapsed. The particle whose Δt is the smallest in the whole device, $\Delta t_{\min}$, is the next one to be moved. After the displacement the private clocks of all other electrons are incremented by $\Delta t_{\min}$. The same is true for the *masterclock*, which is only zeroed once, namely at the very beginning of the simulation. The masterclock displays the simulated time and forms the basis for all current calculations. Synchronous events with respect to the masterclock enter the stage by the following important convention: the private clocks and the masterclock are only incremented when $\Delta t_{min} > 0$ holds true. Mathematically speaking, the presented algorithm generates a semi-Markovian *Continuous Time Random Walk*.

4.2. SIMULATION OF THE BULK AND ITS INTERFACES

In accordance to Bässler's explanation (Bässler 1993) of Gill's law (Gill 1972), the DOS was assumed to be a static Gaussian. The uncorrelated Gaussian disorder model further assumes that neither the mean nor the variance depend on the distances to the organo-metallic heterojunctions. Moreover, the probability densities of spacially neighbored levels are assumed to be uncorrelated. Neglecting activation energies stemming from *polaron binding energies*, the different works necessary for the oxidation and reduction of the molecules' π and π^* levels are viewed to be the sole origin of energetic barriers.

The bulk was modeled as a cubic lattice with a uniform temperature, being traversed by carriers obeying Pauli's exclusion principle. Two isoenergetic orbitals with antiparallel spins form a level, a pair of one bonding and one antibonding level forms a site. Transfer rates to filled levels are equal to zero. The metal contacts are also modeled as jumping sites with an energy equal to the metal's negative work function. The distance separating the electrode from the bulk equaled the lattice constant.

Assuming that the electronic system is a uniformly distributed carrier gas of low density, the influence of long range Coulomb forces between the mobile carriers were neglected and the electric field was approximated by the homogeneous field of a capacitor filled with a dielectric, $\epsilon_0 \epsilon_r E = U/d$. Here, U denotes the applied bias and d the film length. As numerous time-of-flight simulations show (Walker *et al.* 2002), this approximation can be

quite realistic in an organic light emitting diode, where the electrons and holes move through an empty DOS.

Whether π or π^* carriers are injected into a polymer film not only depends on the bulk material in use but also on the device material composition. Since the currents measured in a pure Au/ZnPc/Au device stem from defect electrons injected into the π band at the anode (Gao and Kahn 2002), the HOMO-electrons' Coulomb fields were assumed to be compensated by that of the uncompensated nuclear countercharges and thus were not expected to induce positive image charges at the metal electrodes. The inert positive background charge caused by the nuclear skeleton, however, was assumed to induce negative image charges at the Gold contacts. As a very simple approximation, each simulated electron only felt the image force induced by a positive Coulombic center at the electron's place. The conduction band in the vicinity of the electrodes was bent accordingly.

Effects due to high carrier concentrations have been mimicked by the means of an alternative toy interaction of the Hubbard type (Hubbard 1963). Namely, a short range hard ball repulsion between two electrons was implemented by a constant on-site Coulomb interaction: in the transfer rate to a partially filled level of energy E_j, the target levels's contribution to the Abrahams–Miller rate was enhanced by an additive constant ΔU. If the transfer though was realized, $E + \Delta U$ was taken as the new energy of the doubly occupied level till the next hop-off. As Fig. 4(c) indicates, this caricature of an interaction does not significantly improve the slope of the simulated curves at the current stage of the simulator. The on-level repulsion thus was set to zero in all subsequent investigations.

Photo-induced or injected carrier concentrations are usually small in comparison with the molecule density. The carrier energies then are distributed according to the Boltzmann factor. For increasing concentrations, the Fermi–Dirac distribution becomes dominant. In thin film transistors the carrier densities can become quite high and the mobilities describing their relation with the conductivity can vary up to several orders of magnitude (Tanase *et al.* 2003). To derive the device-specific carrier concentration self-consistently, the simulations started with charging an empty bulk. After a certain carrier concentration in the injection layer had been established, the propagation of carriers along the bulk gained in importance. Current measurements started after the first carrier had successfully traversed the film. After a while, the dynamics perpetuated electron injection, propagation and ejection quite stationarily. After each subhistory the level energies and wave function overlaps were randomized. This step corresponds to a random rotation of each molecule and means that no specific morphology but a whole *class* of films is simulated.

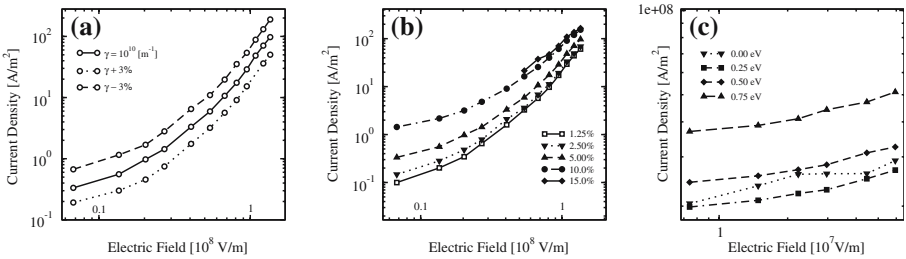

Fig. 4. (a) Shows the effect of varying the conjugation factor and thus the carrier delocalization by ± 3%. (b) Illustrates the two contrary effects of *freezing out* and *diffusion enhancement* when conjugation is a distributed quantity of increasing dispersion Σ. (c) Illustrates the effect of different hard ball repulsions for $2\gamma a = 10$.

5. Results

The goal of the simulator is to reproduce the electrical characteristics of undoped, p-conductive, amorphous Zinc Phthalocyanine films (Gao and Kahn 2002).

The simulations were performed on regular, cubic lattices with an edge length of 10 nm. Figures 4 and 5(a) were generated using a lattice constant of 1 nm, Fig. 5(b) was generated with 0.6 nm. The temperature was set to 300 K. The values for the band structure have been taken from (Gao and Kahn 2002). The value for the attempt-to-escape frequency was set to $\nu_0 = 1.0 \times 10^{12}\,\mathrm{s}^{-1}$ in accordance with (Schmechel 2003).

Figure 4(a) exhibits a quite plausible conduction enhancement for stronger delocalized carriers. The insight from this graph is that variations of the conjugation factor do not alter the qualitative behavior of the device. With respect to the complex reactions possibly taking place at an organo-metallic interface, the assumption of an universal wave function decay throughout the whole device is surely arguable. Figure 4(b) was generated by assuming that not only the energy, but also the conjugation factor γ is a normally distributed random variable of a spread Σ. As Bässler pointed out, this assumption is a quite questionable model for *spacial disorder*. The curves show, that increasing the variance of γ generates more strong than weak orbital overlaps. The case when γ splits into a sum of dispersed site-specific contributions, $\gamma = \gamma_i + \gamma_j$, has not been investigated.

Figure 5(a) depicts the injection efficiency. The Fowler–Nordheim model predicts a straight line, which is clearly not the case for the simulation. Hence, at low electric fields, thermionic emission clearly dominates over tunneling. Qualitatively, this result reproduces the behavior found experimentally as well as the findings of Wolf's simulations (Wolf *et al.* 1999). The curve for $\Sigma = 0.1\gamma$ shows a slight current increase at lower fields. This result could be due to a well-known anomaly (Bässler 1993): increasing the

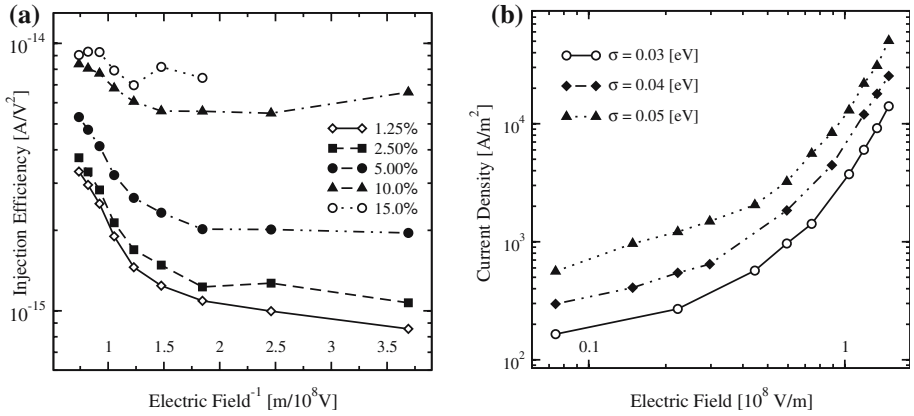

Fig. 5. (a) Injection efficiency in terms of the Fowler–Nordheim model parametric in the spacial disorder parameter Σ. For low fields the characteristics for 10% mirrors the effect of diffusion enhancement. (b) Current–voltage characteristics parametric in σ. The simulated injection current increases due to enhanced disorder in the injection layer.

field can force electrons to avoid the fast channels and move along retarding paths characterized by a poor orbital overlap.

Figure 5(b) was generated with a spacial disorder of Σ = 5%. As far as the bulk transport is concerned, the enhancement of the energy levels' statistical spread increases the mean barrier height and thus the material's electrical resistance. For the specific choice of simulation parameters, however, a current increase for enhanced energetic disorder especially at lower fields is observed. A similar effect was noticed and discussed by Houili and Zuppiroli (2006) when applying KMC techniques to energetic barriers at organic–organic heterojunctions. Namely, this effect could be due to particular *hot spots* where the barrier across the heterojunction is locally lowered. Such points could overcompensate the influence of injection points where the barriers are locally increased.

Figure 6(a) shows that the simulations unfortunately do not replicate the correct conduction regime yet. Namely, the current clearly is thickness dependent and hence shows bulk limited instead of injection limited behavior. Experimentally, such behavior is only found for films p-doped with F_4TCNQ (Gao and Kahn 2002). As Gao shows, the effect of doping results from an improved injection, but does not improve the bulk conductivities. The reason for the ohmic behavior here are the deep interfacial traps in the *undoped* material, which provide more carriers than the bulk can conduct.

Figure 6(b) compares the measured currents with the simulated ones. Since Au/ZnPc/Au exhibits injection-limited behavior, the experimental currents coincide for film thicknesses ranging from 1400 to 7400 Å. The conclusion is essentially the same as for Fig. 6(a), the current's slope especially at high field strengths is magnitudes too low.

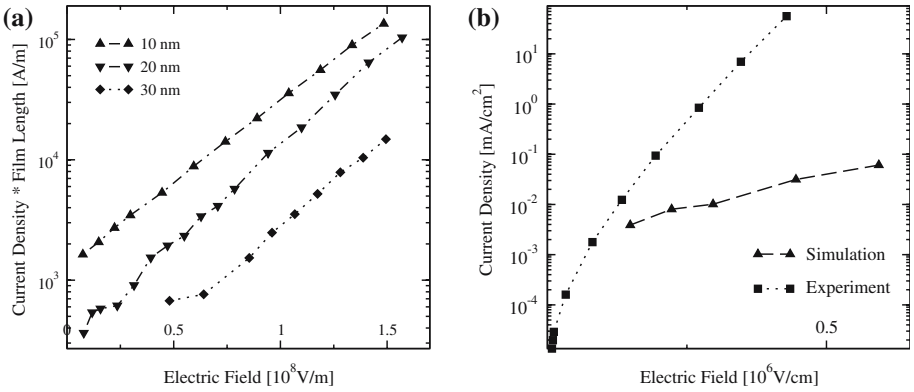

Fig. 6. (a) The simulated transport shows bulk-limited behavior in contrast to the measurements. (b) The simulated current densities compared with the measured ones for an energetically weakly disordered cubic system with an edge length of 10 nm. The simulation parameters are: $a = 0.61$ nm, $2\gamma a = 3.68$, T=300K, $\sigma = 0.05$eV, $\Sigma = 0.15\gamma$.

It is believed that the discrepancy between the simulations and the empirical data is due to the neglection of space charge effects. First, the accumulation of mobile charges at the interfaces are excluded and so were the resulting field-enhancments, which especially arise at interfaces and heterojunctions (Houili and Zuppiroli 2006). On the contrary, due to the missing repulsion from already injected electrons, the injected currents are relatively high at all field strengths and so the current's growth is too small. Secondly, the influence of the immobile charges, i.e., the ionic polymer backbone has been simplified to a single Coulomb potential. The band bending in real films is surely much stronger.

6. Conclusions

When all physical phenomena determining the electrical characteristics of a semiconductor device are based on a common footing, numerical simulations can predict the relevant transport data under quite different conditions. The presented simulator of a p-conductive Gold–Zinc Phthalocyanine–Gold assembly covers self-consistently the injection, propagation and ejection as well as the recombination and excitation of spin $\frac{1}{2}$ particles. Long range as well as short range Coulomb interactions between the mobile carriers have been disregarded. However, the polymer backbone's electrostatic influence on the hopping levels was modeled in a simple way. In consideration of the strong simplifications assumed, the simulated current–voltage curves and injection efficiencies show quite reasonable behavior (Figs. 4 and 5).

Acknowledgment

This work has been supported by the Austrian Science Fund, grant P16862-N02.

References

Bässler H. Phys. stat.sol. (b) **175**(15) 15 1993.
Fichthorn K.A., W.H. Weinberg J. Chem. Phys. **95**(2) 1090 1991.
Gao W., A. Kahn Organic Electronics **3** 53 2002.
Gill W.D. J. Appl. Phys. **43** 5033 1972.
Houili H., L. Zuppiroli J. Appl. Phys. **100**(1) 1 2006.
Hubbard J. Proc. Roy. Soc. **A 276** 238 1963.
Noolandi J. Phys. Rev. B **16** 4474 1977.
Schmechel R. Phys. Rev. B **93**(8) 4653 2003.
Schwoerer M., H.C. Wolf Organische Molekulare Festkörper, Wiley-VCH Verlag Weinheim 2005.
Tanase C., E.J. Meijer, P.W.M. Blom, D.M. de Leeuw Phys. Rev. Lett. **91** 216601 2003.
Walker A.B., A. Kambili, S.J. Martin J. Phys.:Condens.Matter **14** 9825 2002.
Wolf U., V.I. Arkhipov, H. Bässler Phys. Rev. B **49**(11) 7507 1999.